Combined analysis of ^{15}N relaxation data from solid- and solution-state NMR.

Veniamin Chevelkov,† Anastasia V. Zhuravleva,‡ Yi Xue,‡ Bernd Reif,†* Nikolai R. Skrynnikov‡*

† *Forschunginstitut für Molekulare Pharmakologie (FMP), Robert-Rössle-Str. 10, 13125 Berlin, Germany*

‡ *Department of Chemistry, Purdue University, 560 Oval Dr., W. Lafayette, IN 47907-2084, USA*

RECEIVED DATE (automatically inserted by publisher); nikolai@purdue.edu and reif@fmp-berlin.de

Nanosecond time-scale backbone dynamics in proteins has been a subject of much interest. While these motions can be detected by solution ^{15}N relaxation methods,[1] they tend to be masked by the overall protein tumbling. As pointed out by Chen et al., "sometimes nanosecond time scale motions with a corresponding squared order parameter as low as 0.9 can go undetected, even with good quality data available at two magnetic fields".[2] The situation can be improved if relaxation data are augmented by residual dipolar couplings (RDCs).[3] This approach, however, is experimentally demanding and the interpretation is complicated by 'structural noise', lack of absolute reference, and possible coupling between internal dynamics and alignment.[4]

Solid-state methods, on the other hand, are well-suited to detect nanosecond motions. In the absence of overall tumbling, slower forms of internal dynamics provide the most efficient channel of spin relaxation. However, because of experimental limitations it has been difficult to obtain a definitive picture of protein dynamics from the solid-state data alone. For instance, a wide range of effective correlation times, from hundreds of picoseconds to hundreds of nanoseconds, have been reported in the solid-state studies of proteins.[5]

In this communication we undertake a *combined analysis of the solid- and solution-state relaxation data* from a small globular protein, α-spectrin SH3 domain (spc SH3). It is common knowledge that structures of globular proteins as determined in solids and in solution are essentially identical. In fact, crystallographic structures provide the best models for analyzing solution NMR data.[6] Crystal contacts, which involve fluid-like layers formed by outward-pointing side chains,[7] have only limited impact. Taking this notion a step further, we suggest that internal protein dynamics in solids and in solution are also similar (assuming that the solid sample is well hydrated and the measurements are conducted at the same temperature). Note the parallel with the RDC studies where it is also postulated that the interaction with environment does not alter native protein dynamics.

The combined analysis uses ^{15}N R_1, R_2, and NOE data (500, 600 MHz) measured in solution, as well as ^{15}N R_1 rates (600, 900 MHz) measured in solid, see Figure 1. The solution data were recorded using well-established experiments;[8] the solid-state data were obtained using an HSQC-style sequence (Figure S1, Supporting Information (SI)) applied to the deuterated sample with a 10% content of amide protons.[9] In the latter case, deuteration allows for ^{1}H detection at high resolution, alleviates problems arising from proton-driven spin diffusion,[10] and avoids extensive probe heating caused by proton decoupling.

As a first step toward data interpretation, the solution data at two fields were analyzed by means of the R_2/R_1 approach[11] yielding the diffusion parameters τ_R^{iso} =7.55 ns and $D_{||}/D_{\perp}$ =1.22. Consequently, the rotational anisotropy was modeled via the effective correlation times, τ_R^{eff}, assigned to individual NH vectors and to the principal axes of ^{15}N CSA tensors.[12] These τ_R^{eff} values were used as the input for standard Lipari-Szabo analysis[13] (definitions of spectral densities are given in Table S2). The interpretation was (predictably) successful, with the experimental solution-state rates reproduced, on average, to within ±1.5%.

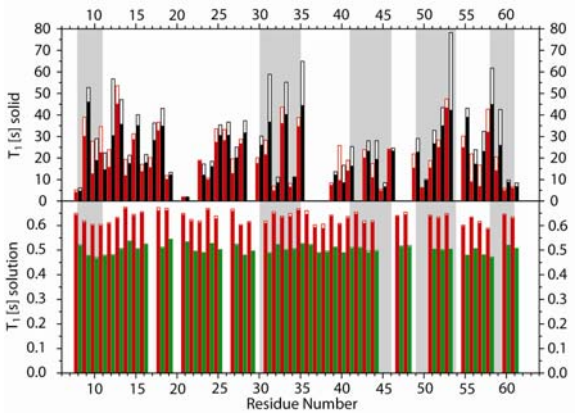

Figure 1. ^{15}N solid- and solution-state T_1 in spc SH3 as measured at 500, 600, and 900 MHz (green, red, and black bars, respectively). The empty portion of each bar corresponds to the experimental uncertainty. Shaded areas in the background indicate β-sheet structure. Sample conditions are listed in Table S1.

The fast-motion parameters S_f^2 and τ_f determined from solution data analysis were subsequently used to predict the solid-state relaxation rates. In doing so, we assumed that fast local dynamics in solids and solution is identical and that it is the only source of relaxation in solids. Accordingly, the spectral densities of the form $J(\omega) = S_f^2\tau_f/(1+\omega^2\tau_f^2)$ were used to calculate solid-state rates. As it turned out, the predicted solid-state R_1 rates were significantly underestimated: on average, they amounted to 0.47 and 0.68 of the experimental rates (600 and 900 MHz, respectively). The discrepancy points toward the presence of additional motional modes that remain undetected in solution. Furthermore, the fact that better agreement is obtained for 900 MHz data suggests that these motions occur on the nanosecond time scale.[14]

In attempt to capture these motions, all data (6 solution and 2 solid rates per residue) were analyzed jointly using the extended Clore-Lipari-Szabo model[1] parameterized with S_s^2, τ_s, S_f^2, and τ_f. In calculating solution rates, τ_R^{iso} was treated as a global variable and adjusted to 7.75 ns. The tumbling anisotropy was accounted for as described above. In calculating solid rates, the contributions from overall tumbling were omitted (Table S2). Following careful optimization, the solution rates were fitted on average to within ±2.1% and the solid rates to within ±3.4%. The outcome of the fitting is illustrated in Figure S2.

It can be readily recognized that the above procedure results in overfitting: indeed, solid-state rates are reproduced far better than can be expected based on the low precision of the measurements (Figure 1). Furthermore, the obtained solutions are not unique. Figure 2a illustrates the typical χ surface in the coordinates S_s^2, τ_s. The long 'valley' appearing in the plot demonstrates that the analysis effectively determines the ratio $(1-S_s^2)/\tau_s$ and fails to separate the two parameters. This is to be expected when solid-state data are limited to R_1 rates and τ_s falls in the macromolecular limit, $\tau_s \gtrsim 10$ ns. Similar behavior has been observed in the pioneering study of Giraud et al.[5d]

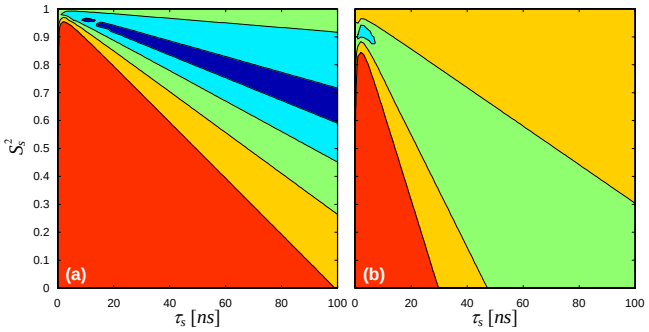

Figure 2. χ surfaces for data from Gln-16 (a) and Leu-8 (b) interpreted by means of the Clore-Lipari-Szabo model. $\chi = <|(\Gamma_i^{fit} - \Gamma_i^{exptl})/\Gamma_i^{exptl}|>$, where Γ_i denotes the complete set of relaxation data, $i = 1..8$, for a given residue. The map is generated by a grid search on S_s^2, τ_s plane, followed by simplex optimization relative to S_f^2, τ_f at each point of the grid. The magnitude of χ is color-coded as follows: <2% (blue), 2-5% (cyan), 5-10% (green), 10-20% (yellow), >20% (red).

The above treatment shows that solid- and solution-state data can be interpreted jointly using the same set of dynamic parameters. To validate this result, we prepared three additional samples of spc SH3 containing 20%, 30%, and 40% w/w of glycerol (see SI for details). Protein molecules in a water-glycerol mixture tend to be surrounded by water[15] and thus retain native-like internal dynamics. The overall tumbling, however, is slowed down (τ_R^{iso} is 11.0, 13.8, and 17.4 ns, respectively), so that slow local motions play a more prominent role in spin-lattice relaxation.[16] As it turns out, R_1, R_2, and NOE data from the three water-glycerol samples can be successfully included in the solid & solution fitting procedure. The result is a credible picture of internal dynamics in the spc SH3. For example, when the optimization is restricted to a (physically reasonable) region $S_s^2 > 0.8$, the solution-state relaxation parameters are reproduced, on average, to within 3.2% and the solid-state rates to within 5.4%. For half of the analyzed residues (17 out of 35) the amplitude of the slow motion turns out to be very small, $S_s^2 > 0.97$ (furthermore, for all but three residues $S_s^2 > 0.92$). The respective correlation times τ_s fall in the interval from 0.8 ns to 54 ns (average 11.5 ns). The fast-motion order parameters S_f^2 range from 0.77 to 0.90 (average 0.83) and τ_f from 0 to 39 ps (average 14 ps). Note, however, that separation of S_s^2 and τ_s remains tentative even with the addition of the new data.

For further corroboration of the method we turned to the MD simulations. A 30-ns trajectory of spc SH3 in explicit solvent was generated using CHARMM equipped with the CMAP module.[17] The correlation functions were extracted in a standard fashion (with the overall tumbling subtracted out)[18] and used to predict the solid-state ^{15}N R_1 rates. While the agreement on a per-residue basis was poor, roughly one half of the simulated rates turned out to be overestimated and another half underestimated (Figure S3). Thus, small-amplitude ns motions observed in solution can, in principle, account for the relaxation rates measured in solids.

Several conclusions can be reached on the basis of the presented results. (i) Fast (ps) motions are responsible for a significant portion of backbone R_1 rates in solids, while the remainder comes from ns dynamics. (ii) Small-amplitude ns motions observed in solids are likely to be present also in solution. (iii) The combined analysis of solid- and solution-state relaxation data provides a promising tool for detailed characterization of ps-ns motions in the protein backbone. Such combined analysis can be strengthened by the addition of new solid-state relaxation experiments.[19] In particular, if the data set is complemented with solid R_2-type data (e.g., transverse cross-correlations[20]) the reliable separation of S_s^2 and τ_s can be effected. It is expected that the proposed approach will provide new and stimulating insights into protein dynamics.

Acknowledgements. We are grateful to Flemming Hansen and Lewis Kay for help with 500 MHz measurements and to the anonymous reviewer for suggesting water-glycerol experiments.

Supporting Information Available: Solid-state pulse sequence for measuring ^{15}N R_1 relaxation; table of solid- and solution-state relaxation rates; expressions for spectral densities; figure illustrating data fitting with Clore-Lipari-Szabo model; comparison of the experimental and MD-simulated R_1 rates in solids; comparison of the experimental and predicted R_1 rates in the water-glycerol solution; table of S_s^2, τ_s, S_f^2, τ_f. This material is available free of charge via the Internet at http://pubs.acs.org

References

(1) Clore, G. M.; Szabo, A.; Bax, A.; Kay, L. E.; Driscoll, P. C.; Gronenborn, A. M. *J. Am. Chem. Soc.* **1990,** *112*, 4989-4991.
(2) Chen, J. H.; Brooks, C. L.; Wright, P. E. *J. Biomol. NMR* **2004,** *29*, 243-257.
(3) (a) Lakomek, N. A.; Farès, C.; Becker, S.; Carlomagno, T.; Meiler, J.; Griesinger, C. *Angew. Chem. Int. Ed.* **2005,** *44*, 7776-7778. (b) Bouvignies, G.; Bernado, P.; Meier, S.; Cho, K.; Grzesiek, S.; Brüschweiler, R.; Blackledge, M. *Proc. Natl. Acad. Sci. USA* **2005,** *102*, 13885-13890.
(4) (a) Zweckstetter, M.; Bax, A. *J. Biomol. NMR* **2002,** *23*, 127-137. (b) Clore, G. M.; Schwieters, C. D. *J. Am. Chem. Soc.* **2004,** *126*, 2923-2938.
(5) (a) Cole, H. B. R.; Torchia, D. A. *Chem. Phys.* **1991,** *158*, 271-281. (b) North, C. L.; Cross, T. A. *Biochemistry* **1995,** *34*, 5883-5895. (c) Mack, J. W.; Usha, M. G.; Long, J.; Griffin, R. G.; Wittebort, R. J. *Biopolymers* **2000,** *53*, 9-18. (d) Giraud, N.; Blackledge, M.; Goldman, M.; Böckmann, A.; Lesage, A.; Penin, F.; Emsley, L. *J. Am. Chem. Soc.* **2005,** *127*, 18190-18210.
(6) Bax, A. *Protein Sci.* **2003,** *12*, 1-16.
(7) Zhou, Y. Q.; Vitkup, D.; Karplus, M. *J. Mol. Biol.* **1999,** *285*, 1371-1375.
(8) Farrow, N. A.; Muhandiram, R.; Singer, A. U.; Pascal, S. M.; Kay, C. M.; Gish, G.; Shoelson, S. E.; Pawson, T.; Forman-Kay, J. D.; Kay, L. E. *Biochemistry* **1994,** *33*, 5984-6003.
(9) Chevelkov, V.; Rehbein, K.; Diehl, A.; Reif, B. *Angew. Chem. Int. Ed.* **2006,** *45*, 3878-3881.
(10) Giraud, N.; Blackledge, M.; Böckmann, A.; Emsley, L. *J. Magn. Reson.* **2007,** *184*, 51-61.
(11) Tjandra, N.; Feller, S. E.; Pastor, R. W.; Bax, A. *J. Am. Chem. Soc.* **1995,** *117*, 12562-12566.
(12) Lee, L. K.; Rance, M.; Chazin, W. J.; Palmer, A. G. *J. Biomol. NMR* **1997,** *9*, 287-298.
(13) Lipari, G.; Szabo, A. *J. Am. Chem. Soc.* **1982,** *104*, 4546-4559.
(14) The contribution from ns motions into R_1 is reduced at the higher field.
(15) Gekko, K.; Timasheff, S. N. *Biochemistry* **1981,** *20*, 4667-4676.
(16) Korchuganov, D. S.; Gagnidze, I. E.; Tkach, E. N.; Schulga, A. A.; Kirpichnikov, M. P.; Arseniev, A. S. *J. Biomol. NMR* **2004,** *30*, 431-442.
(17) Buck, M.; Bouguet-Bonnet, S.; Pastor, R. W.; MacKerell, A. D. *Biophys. J.* **2006,** *90*, L36-L38.
(18) Chandrasekhar, I.; Clore, G. M.; Szabo, A.; Gronenborn, A. M.; Brooks, B. R. *J. Mol. Biol.* **1992,** *226*, 239-250.
(19) Giraud, N.; Sein, J.; Pintacuda, G.; Böckmann, A.; Lesage, A.; Blackledge, M.; Emsley, L. *J. Am. Chem. Soc.* **2006,** *128*, 12398-12399.
(20) (a) Chevelkov, V.; Faelber, K.; Schrey, A.; Rehbein, K.; Diehl, A.; Reif, B. *J. Am. Chem. Soc.* **2007,** *129*, 10195-10200. (b) Skrynnikov, N. R. *Magn Reson Chem* **2007,** *submitted*.

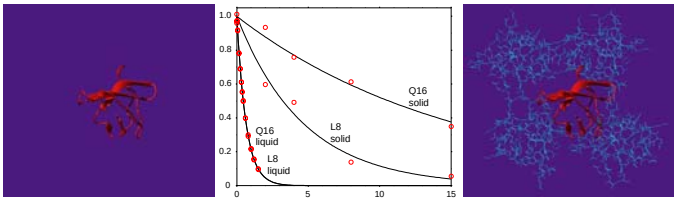

It is well known that structures of globular proteins in liquid and in crystalline solid are essentially identical. Many lines of evidence suggest that internal dynamics are also similar (assuming that the solid sample is well hydrated and the measurements are conducted at the same temperature). Based on this premise, we undertake a combined analysis of solid- and liquid-state ^{15}N relaxation data from a small globular protein, α-spectrin SH3 domain. The interpretation using the extended Lipari-Szabo model demonstrates that liquid R_1, R_2, NOE and solid R_1 data measured at multiple fields are mutually consistent. To validate these results, we prepared a series of samples where the protein is dissolved in a water-glycerol solvent. The presence of glycerol ensures that the overall protein tumbling is slowed down, thus increasing the visibility of nanosecond time-scale internal motions. When additional data are included in the fitting procedure, a credible picture of protein dynamics is obtained. In particular, the analysis suggests that ns time-scale motions with very low amplitude, S^2~0.95, are present throughout the protein. It is envisaged that combined analyses of liquid- and solid-state data can provide a powerful method for detailed characterization of internal dynamics in proteins at multiple time scales.

Supporting Information

Combined analysis of ^{15}N relaxation data from solid- and solution-state NMR.

Veniamin Chevelkov,[†] Anastasia V. Zhuravleva,[‡] Yi Xue,[‡] Bernd Reif,[†]* Nikolai R. Skrynnikov[‡]*

† *Forschunginstitut für Molekulare Pharmakologie (FMP), Robert-Rössle-Str. 10, 13125 Berlin, Germany*

‡ *Department of Chemistry, Purdue University, 560 Oval Dr., W. Lafayette, IN 47907-2084, USA*

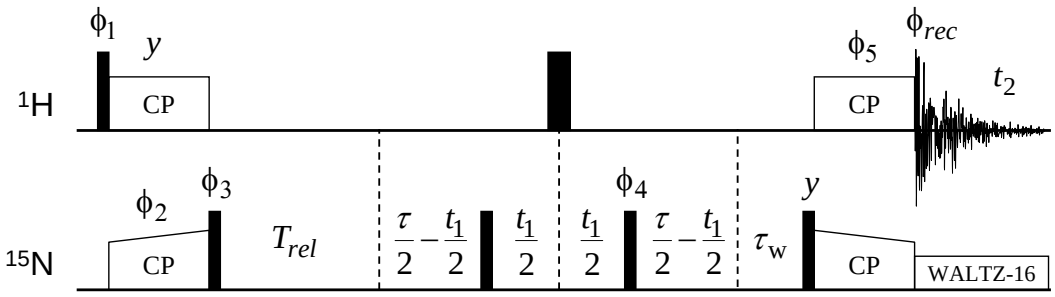

Figure S1. A solid-state NMR experiment for measuring backbone ^{15}N R_1 relaxation. The sequence was designed for application to the deuterated samples with a low content (ca. 10%) of protons in amide positions. Narrow (wide) pulses were applied with a flip angle of 90° (180°). The *rf* carriers were set at 4.94 (HDO line) and 119 ppm for ^{1}H and ^{15}N, respectively. The hard pulses on ^{1}H and ^{15}N channels were applied with the field strengths of 60 and 50 kHz, respectively. WALTZ-16 decoupling[1] on ^{15}N channel was applied for 100 ms with the field strength of 2 kHz. During the CP elements, constant rf power of 54 kHz was applied on ^{1}H channel, while the rf power on the nitrogen channel was swept from 36 to 45 kHz, achieving a frequency match at (-1) spinning sideband.[2,3] The duration of the CP element was 0.8 ms. A variant of the constant-time scheme proposed by Zilm and co-workers[4] with τ = 26 ms, τ_w = 60 – 120 ms was used to improve water suppression (note that due to long nitrogen T_1 the loss of magnetization during $\tau - t_1 + \tau_w$ is negligible). The decay curves were sampled using T_{rel} of 0, 2, 4, 8, and 15 s or, alternatively, 0, 2, 4, 7, and 13 s (600 and 900 MHz data, respectively). The recycling delay between the two consecutive scans was 2.0 s. The spectral width in ^{1}H dimension was 50000 Hz, the spectral width in ^{15}N dimension was 1800 (2700) Hz at 600 (900) MHz static field. The rf pulses have been applied with the phase x, unless indicated otherwise. The phase cycle was $\phi1$ = (x,-x), $\phi2$ = 2(x)2(-x), $\phi3$ = 4(y)4(-y), $\phi5$ = 8(x)8(-x), ϕ_{rec} =(x,-x,-x,x,-x,x,x,-x,-x,x,x,-x,x,-x,-x,x). Phase-sensitive detection in t_1 was achieved by TPPI[5] of $\phi4$. The total experimental time at 600 (900) MHz was 125 (180) h. The moderate MAS frequency, 13 kHz, was used to avoid sample degradation during the long experimental run.

Table S1. The summary of experimental relaxation data

Residue	R_1(500)	R_2(500)	noe(500)	R_1(600)	R_2(600)	noe(600)	R_1^{solid}(600)	R_1^{solid}(900)
8	1.924	9.272	0.723	1.548	9.818	0.713	0.2150	0.1865
9	2.095	9.617	0.743	1.624	10.060	0.784	0.0290	0.0203
10	2.134	9.904	0.822	1.660	10.387	0.820	0.0494	0.0418
11	2.095	10.223	0.761	1.662	10.722	0.798	0.0351	0.0541
12	2.086	10.060	0.738	1.642	10.589	0.810	0.0505	0.0230
13	1.982	9.500	0.771	1.587	10.064	0.758	0.0203	0.0242
14	1.868	8.825	0.716	1.489	9.408	0.746	0.0642	0.0517
15	1.984	9.381	0.767	1.557	10.007	0.763	0.0334	0.0266
16	1.912	9.263	0.724	1.531	9.914	0.772	0.0651	0.0507
18	1.963	9.355	0.729	1.501	10.108	0.762	0.0289	0.0257
19	1.843	8.986	0.656	1.503	9.501	0.691	0.0907	0.0785
21	1.876	8.875	0.692	1.547	9.689	0.689	0.5293	0.5327
23	2.043	9.531	0.767	1.625	10.580	0.755	0.0534	0.0684
24	1.903	8.497	0.728	1.500	9.137	0.750	0.0971	0.0580
25	1.995	10.083	0.740	1.580	10.840	0.779	0.0329	0.0304
27	1.916	10.003	0.746	1.509	10.772	0.746	0.0617	0.0443
28	2.089	9.709	0.740	1.663	10.396	0.778	0.0361	0.0290
31	2.053	9.481	0.750	1.629	10.140	0.779	0.0402	0.0209
32	1.920	8.929	0.740	1.535	9.565	0.712	0.1713	0.1015
33	2.000	10.409	0.784	1.575	11.124	0.785	0.0251	0.0210
34	1.985	10.461	0.780	1.556	10.954	0.811	0.1350	0.0902
35	1.906	9.479	0.741	1.504	9.954	0.805	0.0272	0.0183
39	1.957	8.395	0.738	1.563	9.399	0.734	0.1273	0.0776
40	2.051	9.368	0.763	1.649	9.244	0.744	0.0564	0.0798
41	1.965	9.039	0.727	1.582	9.601	0.776	0.0607	0.0482
43	2.026	9.763	0.760	1.629	9.921	0.775	0.0456	0.0391
44	2.015	10.558	0.775	1.623	11.237	0.793	0.0706	0.0422
51	1.986	10.048	0.770	1.562	10.687	0.793	0.0584	0.0337
52	2.001	9.621	0.735	1.583	10.284	0.766	0.0375	0.0255
53	1.989	10.074	0.805	1.551	10.662	0.781	0.0220	0.0166
55	2.094	10.532	0.790	1.669	11.253	0.770	0.0363	0.0244
56	1.979	10.049	0.735	1.582	10.796	0.804	0.0648	0.0488
57	2.085	9.478	0.769	1.633	10.111	0.795	0.0852	0.0361
58	2.129	10.301	0.785	1.705	11.041	0.789	0.0268	0.0187
60	1.928	9.065	0.738	1.552	9.638	0.770	0.1860	0.1075
61	1.980	8.555	0.639	1.583	8.907	0.645	0.1574	0.1313

The sample of SH3 domain from chicken α-spectrin used in solution measurements was prepared with u(^{13}C,^{15}N),50%-^{2}H labeling scheme using glucose as the sole carbon source. The sample conditions were 90% H_2O – 10% D_2O, pH=3.5, unbuffered; the experiments were conducted at 7.0±0.2 ºC. The sample employed in the solid-state measurements was prepared with u(^{15}N,^{2}H) labeling scheme using glycerol as a sole carbon source. The protein was crystallized from 10% H_2O – 90% D_2O solvent, pH 7, as described previously.[6] The material was mechanically transferred from the crystallization bath to a 3.2 mm rotor. The actual pH of the solid-state sample containing a relatively small amount of water is largely uncertain. The sample temperature during the solid-state measurements was estimated to be 10.0±3.0 ºC.

Only those residues for which all eight pieces of data are available are included. The average errors for the data listed above (left to right) are 0.4, 0.6, 1.5, 0.6, 1.0, 0.8, 15.0 and 15.0 %. These errors

are obtained from the exponential fitting of the decay curves (in the case of NOE the previously described approach has been used[7]). The errors evaluated in this manner are usually underestimated by approximately a factor of 2 relative to the errors based on repeat measurements.

In addition to a large random error, the solid-state rates may be prone to certain biases. First, the exchange of amide protons with water and substitution of ^{2}H for ^{1}H during the long delay T_{rel} may lead to the increased apparent relaxation rates. This effect is not dominant as evidenced by the fact that (*i*) the decay rates in β-sheet residues, which are protected from exchange, are similar to those outside the secondary structure and (*ii*) the measured decay rates show a pronounced field dependence which is characteristic of relaxation, but not of exchange. Since the effective pH of the solid sample remains uncertain, it is difficult to quantify the effect of exchange. The additional experiments are currently underway to address this problem.

Second, it was recently observed that ^{15}N-^{15}N spin diffusion persists at moderately high MAS rates.[8] In particular, magnetization leakage from backbone nitrogen to methyl-like NH_3 groups from Lys side chains leads to higher-then-expected apparent relaxation rates. We believe that our experimental scheme is relatively safe in this regard. Indeed, NH_3 can be an efficient relaxation sink[9] for the backbone NH moieties, whereas ND_3 can be an efficient sink for ND groups. However, ND_3 will not be an efficient sink for the NH groups. This latter observation applies to our experimental study which uses the sample crystallized from 10% H_2O – 90% D_2O solvent. Analysis of the crystallographic structure of α-spectrin SH3 demonstrates that there is no correlation between the measured solid-state R_1 rates and the proximity to NH_3 groups.

Third, no attempt was made to suppress ^{1}H-^{15}N dipolar – ^{15}N CSA cross-correlations[10,11] during the experiment Fig. S1. Using the N_z relaxation rates listed above, as well as H_z and $2H_zN_z$ relaxation rates experimentally measured in the same solid-state sample (ca. 0.3 and 4.0 s^{-1}, respectively) and assuming the same set of T_{rel} as used in the experiment Fig. S1, we estimated that the effect of cross-correlations on the measured rates typically does not exceed 2%. This is well below the level of experimental uncertainty. In this connection we note that the fast decay of the $2H_zN_z$ mode (attributed to selective proton relaxation) leads to 'self-decoupling' effect and suppression of cross-correlations.

In conclusion, it should be recognized that the solid-state data are loaded with substantial error, attributable mainly to poor signal-to-noise ratio, but also to certain systematic factors. In the future, the improvements in instrumentation and experimental designs will allow for more accurate measurements.

Table S2. Model-free correlation functions $g(t)$ and spectral densities $J(\omega)$ for analysis of spin relaxation in solids and solution.

	Solution	Solid
Lipari-Szabo model[12]	$g(t) = \{S_f^2 + (1-S_f^2)e^{-t/\tau_f}\}e^{-t/\tau_R^{eff}}$ $J(\omega) = S_f^2 \frac{\tau_R^{eff}}{1+(\omega\tau_R^{eff})^2} + (1-S_f^2)\frac{\tau}{1+(\omega\tau)^2}$ $1/\tau = (1/\tau_f) + (1/\tau_R^{eff})$	$g(t) = (1-S_f^2)e^{-t/\tau_f}$ $J(\omega) = (1-S_f^2)\frac{\tau_f}{1+(\omega\tau_f)^2}$
Clore-Lipari-Szabo model[13]	$g(t) = \{S_f^2 + (1-S_f^2)e^{-t/\tau_f}\}\times$ $\{S_s^2 + (1-S_s^2)e^{-t/\tau_s}\}e^{-t/\tau_R^{eff}}$ $J(\omega) = S_f^2 S_s^2 \frac{\tau_R^{eff}}{1+(\omega\tau_R^{eff})^2} + S_f^2(1-S_s^2)\frac{\tau_1}{1+(\omega\tau_1)^2} +$ $(1-S_f^2)S_s^2 \frac{\tau_2}{1+(\omega\tau_2)^2} + (1-S_f^2)(1-S_s^2)\frac{\tau_3}{1+(\omega\tau_3)^2}$ $1/\tau_1 = (1/\tau_s) + (1/\tau_R^{eff})$ $1/\tau_2 = (1/\tau_f) + (1/\tau_R^{eff})$ $1/\tau_3 = (1/\tau_f) + (1/\tau_s) + (1/\tau_R^{eff})$	$g(t) = \{S_f^2 + (1-S_f^2)e^{-t/\tau_f}\}\times$ $\{S_s^2 + (1-S_s^2)e^{-t/\tau_s}\}$ $J(\omega) = S_f^2(1-S_s^2)\frac{\tau_s}{1+(\omega\tau_s)^2} +$ $(1-S_f^2)S_s^2 \frac{\tau_f}{1+(\omega\tau_f)^2} + (1-S_f^2)(1-S_s^2)\frac{\tau}{1+(\omega\tau)^2}$ $1/\tau = (1/\tau_f) + (1/\tau_s)$

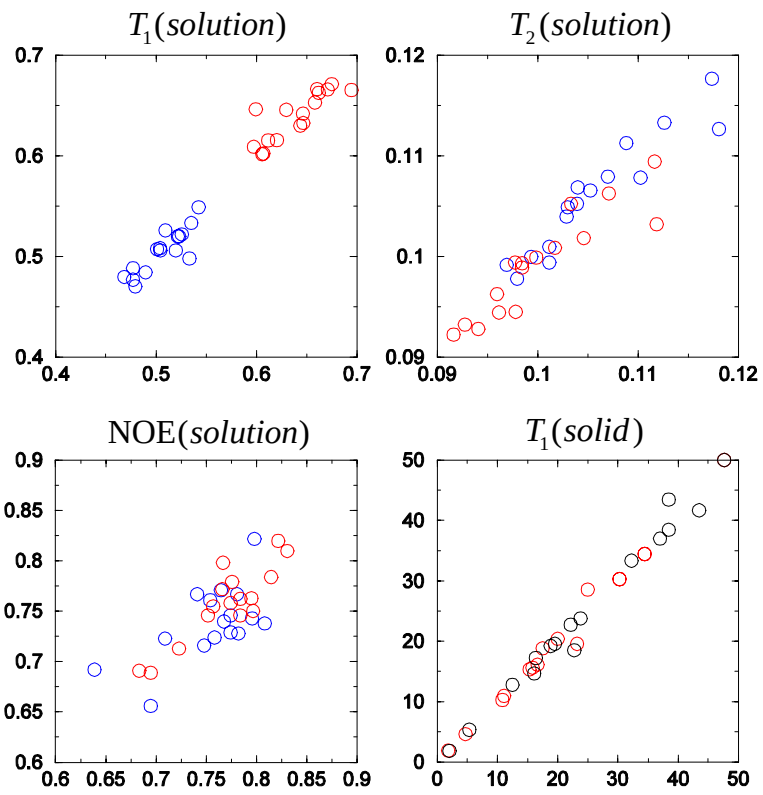

Figure S2. The results of the combined analysis of solid- and solution-state ^{15}N relaxation data using the extended model-free model.[13] The data are from 500 (blue), 600 (red), and 900 (black) MHz measurements. In each panel, the experimental values are plotted along the *y* axis and the best-fit values along the *x* axis. The mean absolute-value deviations between the measured and the fitted rates amount to 1.5%, 1.5%, and 3.4% for the solution T_1, T_2, and NOE panels, respectively, and 3.7 % for the solid T_1 data. The latter value is much lower than the experimental uncertainty associated with solid-state T_1, indicative of overfitting. Note that the least-square fitting has been performed on the rates R_1, R_2 as described in the text. However, for the purpose of plotting the results were converted into T_1, T_2 and the deviations were re-calculated accordingly.

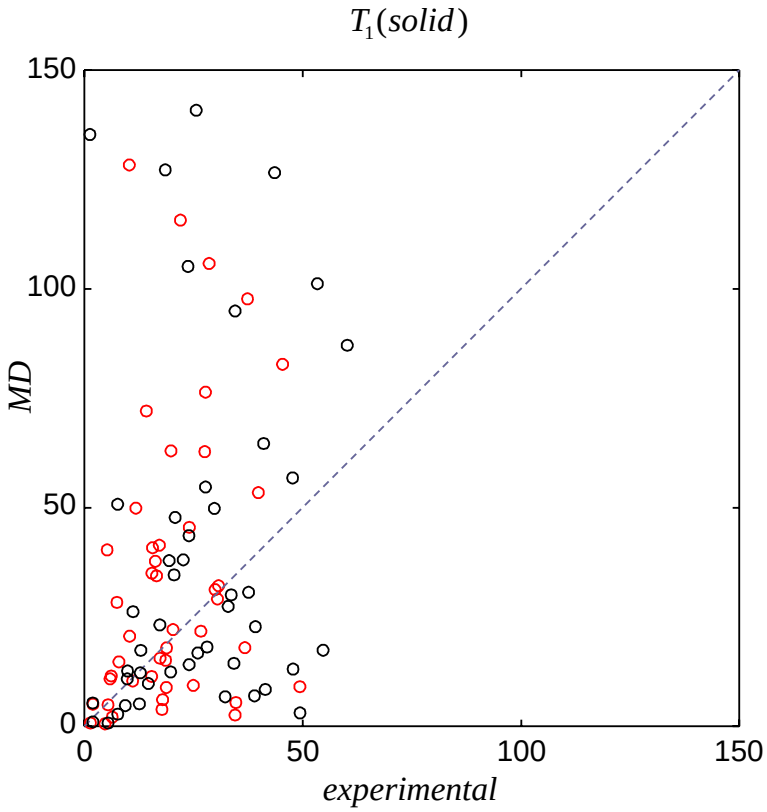

Figure S3. Comparison of the experimental solid-state T_1 data with predictions from the MD simulations (600 MHz: red; 900 MHz: black). The MD trajectory has been recorded with the program CHARMM[14] version 32b2 equipped with the CMAP module[15] using the standard liquid-state protocol described by Yi et al.[16] The modifications to the previously described procedure are as follows: (*i*) six N-terminal residues and one C-terminal residue missing from the crystallographic coordinates have been added to the structure and subjected to energy minimization prior to the equilibration and production run; the water box was constructed to accommodate the extended N-terminal tail, (*ii*) the protonation status of Asp and Glu side-chain carboxylic groups was adjusted by means of the program PROPKA[17] assuming pH 3.5. The role of the CMAP module is to supply the corrections to the energy term associated with ϕ/ψ dihedral angles. This module has been shown to significantly improve the modeling of backbone dynamics.[15] The duration of the trajectory was 30 ns at the nominal temperature of 20 ºC. The solid-state T_1 values were predicted from the MD data using the numerically accurate representation of the correlation functions as described by Yi et al.[16] Of all predicted T_1 values, 51 are too long (lie above the diagonal) and 41 are too short (below the diagonal). Note that the relatively short 30-ns trajectory cannot be expected to accurately model the nanosecond time-scale internal dynamics. This must be in part responsible for the considerable scatter observed in the plot.

Relaxation measurements using glycerol-water mixture as a solvent.

In solution, ^{15}N relaxation is dominated by the overall protein tumbling. On the contrary, in solids protein tumbling is abrogated,[18] so that nitrogen relaxation turns out to be sensitive to the internal motions on the time scale $\gtrsim 1$ ns. It is also possible to create an 'intermediate' situation where the overall tumbling is slowed down, yet not completely abolished. This can be achieved simply by adding a viscogen, such as glycerol, to a water-based solution sample. It is expected that the effects of ns time-scale internal dynamics can be somewhat emphasized in this fashion.[19-21]

A mixture of water and glycerol is a protein-friendly solvent, which is especially well known for its cryoprotectant properties.[22] Protein molecules in a water-glycerol mixture tend to be surrounded by water, whereas bulk solvent contains a higher proportion of the glycerol.[23,24] This leads to a favorable situation where the protein can be observed in a native-like environment. However, when the concentration of glycerol is increased (approaching pure glycerol) the native character of protein dynamics can be altered.[25] Furthermore, the increasingly long protein rotational correlation time τ_R makes it difficult to accurately measure ^{15}N relaxation. This imposes a practical limit on the scope of studies using a water-glycerol solvent.

For our study we used the sample of spc SH3 with u(^{13}C,^{15}N),50%-^{2}H labeling scheme. The solvent was prepared by adding 20% (30%, 40%) w/w of d_5-glycerol (Sigma) to water (unbuffered, pH pre-adjusted to 3.5). The chemical shifts were very similar (although not identical) to those observed in the water solution. The ^{15}N R_1, $R_{1\rho}$, and saturation-transfer measurements were conducted at the magnetic field of 600 MHz using a standard set of experiments[26-28] with appropriately adjusted durations of the relaxation period, evolution period, and recycling delay. The measured R_1 values are plotted in Fig. S4 in a form of a blue band which corresponds to the $R_1 \pm 2\%$ corridor (here 2% is a generic estimate for the experimental error).

We further attempted to compare the R_1 data obtained from water-glycerol samples with the predictions from our prior analyses. The underlying assumption in this approach is that the internal protein dynamics in the water-glycerol solvent is no different from that in pure water (either in solution, or in crystalline phase). Based on this assumption, we combined the previously derived S_f^2, τ_f, S_s^2, τ_s values with the overall tumbling time τ_R^{iso} characteristic of the water-glycerol mixture. On this basis, we predicted the expected R_1 rates for the water-glycerol samples (red circles in Fig. S4).

Specifically, the analyses were conducted as follows. First, τ_R^{iso} values were determined for spc SH3 in the water-glycerol solvent. For this purpose, only the residues with NOE>0.70 in the water-glycerol mixture were retained in the data set.[29] The resulting reduced data set was used to perform the R_2/R_1-type analysis,[29] where the anisotropy parameter $D_{\|}/D_{\perp}$ and the orientation of the diffusion tensor long axis were *fixed* according to our previous findings (see main text) while $\tau_R^{iso}(=1/6D_{iso})$ was optimized. This procedure produced good-quality fits and resulted in τ_R^{iso} values of 11.0, 13.8, and 17.4 ns for 20%-, 30%, and 40%-glycerol solvent, respectively. The obtained values of τ_R^{iso} were used to calculate

τ_R^{eff} for each individual NH vector[30] and, separately, for each CSA vector (corresponding to the unique axis of the presumed axially-symmetric ^{15}N CSA tensor).

As a next step, we combined the obtained τ_R^{eff} values with S_f^2, τ_f, S_s^2, and τ_s derived from our previous Clore-Lipari-Szabo treatment of the solid and solution data (see main text). All these parameters can be inserted in the Clore-Lipari-Szabo formula (Tab. S2) to predict the ^{15}N R_1 values expected for the water-glycerol samples. The results are presented in Fig. S4, panels A-C. In this connection one should keep in mind that the presence of nanosecond time-scale local dynamics leads to underestimation of τ_R^{iso} by the R_2/R_1-type analysis. Indeed, if the values of τ_R^{iso} are adjusted slightly upward the agreement between the predicted and the experimental R_1 rates improves (Fig. S4, panels D-F).

The inspection of Fig. S4 suggests that our previous analysis (including the identification of small-amplitude ns dynamics) is broadly consistent with the data from the water-glycerol samples. One clear exception is residue 21 which appears as an outlier in the plot. In our prior treatment we determined that there is a substantial amount of nanosecond dynamics in this residue ($S_s^2 = 0.77$, $\tau_s = 1.7$ ns). This result has been, however, suspect since the quality of fitting for this particular residue was among the poorest and the χ^2 surface showed two disjointed minima. The present set of data from the water-glycerol samples demonstrates that the presence of nanosecond time-scale dynamics was most probably overestimated in this case. It is also possible that the presence of glycerol causes a change in the native dynamics at this particular site (which belongs to the loop region). For other residues, however, there is a reasonable agreement between the experimental and the predicted R_1 values.

To further emphasize the consistency of the results, we undertook a comprehensive analysis of all available relaxation data: 6 solution datasets from the aqueous sample, 2 solid-state datasets, plus 9 solution datasets from a series of water-glycerol samples. The fitting was carried out using the extended Clore-Lipari-Szabo model in the same fashion as described in the main text (see also Fig. S2). Two modifications were made to the fitting procedure to make it more restrictive. First, the correlation times τ_R^{iso} were used directly as obtained from R_2/R_1-treatment without any further adjustment. Second, the search was restricted to the region $S_s^2 > 0.8$ thus imposing a (physically reasonable) limit on the amplitudes of slow motions. The fitting executed under these conditions proved to be successful: the solution-state relaxation parameters were reproduced to within 3.2% (mean absolute-value deviation), whereas the solid-state rates were reproduced to within 5.4%. Furthermore, a very reasonable set of dynamic parameters has been obtained, Tab. S3. Specifically, for half of the analyzed residues (17 out of 35) the amplitude of the slow motion is very small, $S_s^2 > 0.97$. In fact, for all but three residues it has been found that $S_s^2 > 0.92$. The corresponding correlation times τ_s vary from 0.8 ns to 54 ns, with the average value equal to 11.5 ns. At the same time, the fast-motion order parameters S_f^2 are in the range from 0.77 to 0.90 (average value 0.83), and τ_f values are distributed between 0 and 39 ps (average value 14 ps). Note, however, that localization of the minimum on the χ-surface remains poor (cf. Fig. 2) so that these results cannot be regarded as definitive.

In evaluating our experience with water-glycerol samples a few cautionary comments should be made. First of all, the experimental error increases substantially with increase in τ_R^{iso} (for instance, the NOE measurement error increases from 2.2% to 3.8% in going from 20%- to 40%-glycerol sample). Second, the modeling of tumbling anisotropy for all solution-state samples, including water-glycerol samples, introduces a potentially significant source of error. Finally, even a substantial (two-fold) increase in the overall tumbling time achieved by use of the water-glycerol solvent is of limited benefit for the analysis of nanosecond dynamics. Indeed, even under these re-defined conditions the R_1 relaxation is dominated, far and away, by the overall protein tumbling.[21,31] In this sense, the solid-state data remain a uniquely attractive source of information since they truly highlight the slower forms of internal dynamics.

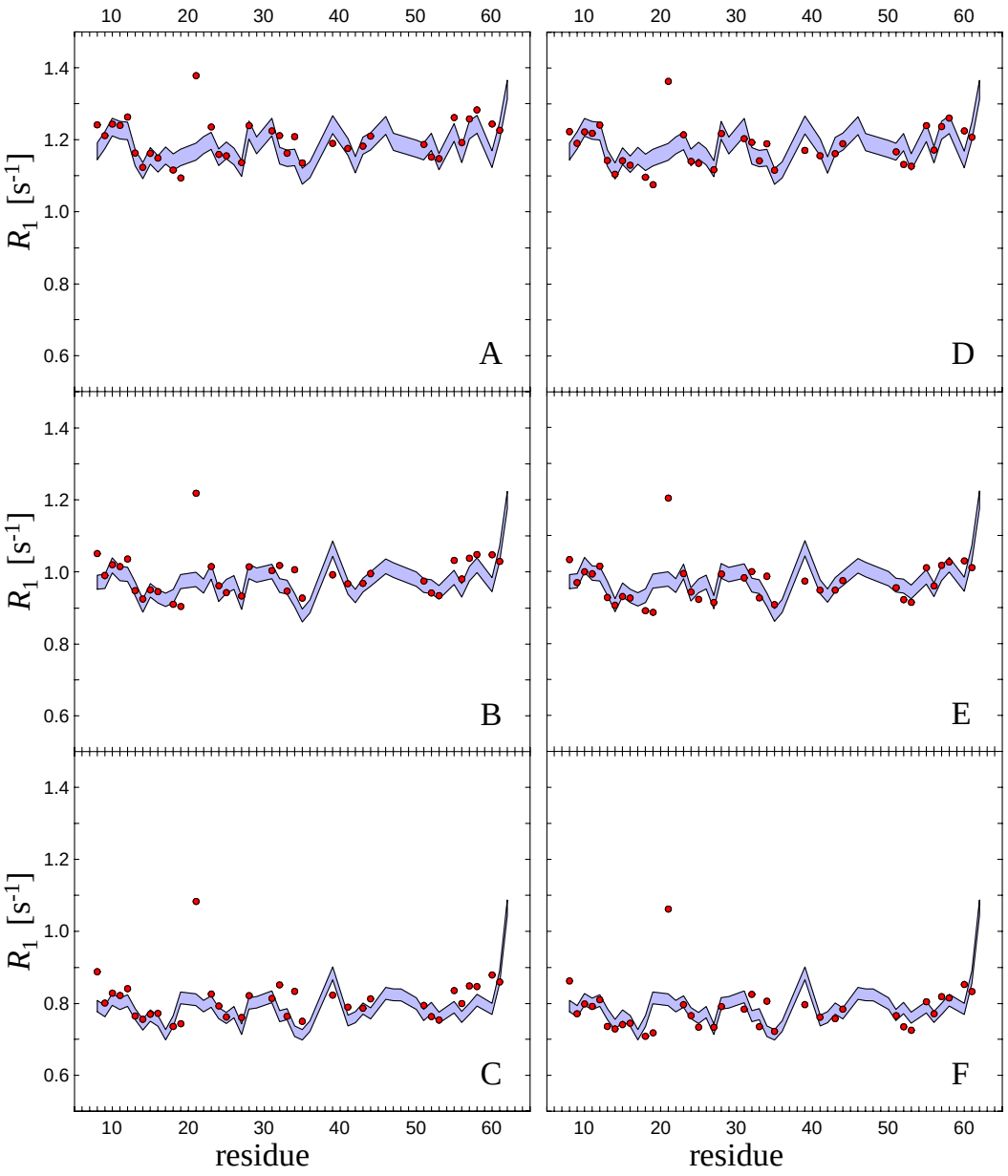

Figure S4. ^{15}N R_1 relaxation rates from the samples of spc SH3 dissolved in the water-glycerol mixture (panels A, D: 20% w/w glycerol; panels B, E: 30% w/w glycerol; panels C, F: 40% w/w glycerol;). The experimentally measured rates are represented via a blue band which corresponds to the $R_1 \pm 2\%$ corridor. The predicted rates, as calculated on the basis of the extended Clore-Lipari-Szabo model, are indicated by the red circles. In the calculations, the overall tumbling correlation times τ_R^{iso} have been used as determined from the R_2 / R_1-type analysis: 11.0, 13.8, and 17.4 ns (panels A-C). Alternatively, τ_R^{iso} values were adjusted to maximize the agreement between the measured and predicted R_1 values in the plot: 11.2, 14.1, and 18.1 ns (panels D-F).

Table S3. Dynamics parameters extracted from the combined analysis of the relaxation data from the solids and solutions (water and water-glycerol samples)

Residue	S_s^2	τ_s [ns]	S_f^2	τ_f [ps]	Deviation(*) [%]
8	0.92	1.9	0.81	22	*4.6*
9	0.97	20.7	0.85	9	*2.9*
10	0.98	2.1	0.87	0	*2.1*
11	0.98	0.8	0.89	4	*4.0*
12	0.93	20.1	0.88	0	*5.6*
13	0.99	0.8	0.83	12	*1.8*
14	0.98	5.0	0.77	17	*2.2*
15	0.98	11.1	0.82	14	*1.8*
16	0.97	6.8	0.80	19	*1.5*
18	0.99	8.2	0.82	16	*2.0*
19	0.80(**)	53.9	0.79	39	*2.8*
21	0.80(**)	1.4	0.83	0	*11.1*
23	0.97	0.8	0.87	8	*4.0*
24	0.93	13.2	0.77	19	*3.7*
25	0.99	2.6	0.86	16	*1.6*
27	0.97	7.4	0.83	17	*2.9*
28	0.99	7.2	0.86	18	*2.4*
31	0.94	23.4	0.86	3	*4.5*
32	0.92	6.8	0.78	24	*4.4*
33	0.99	9.1	0.87	15	*1.5*
34	0.95	4.3	0.84	17	*5.0*
35	0.99	4.6	0.80	0	*3.5*
39	0.80(**)	27.0	0.79	25	*3.7*
41	0.98	4.9	0.81	18	*2.4*
43	0.99	5.4	0.84	23	*1.8*
44	0.96	7.5	0.89	3	*3.3*
51	0.93	18.9	0.85	10	*3.4*
52	0.93	36.1	0.85	12	*2.9*
53	0.96	34.9	0.85	9	*1.6*
55	0.97	13.2	0.89	15	*3.9*
56	0.98	6.2	0.85	21	*2.4*
57	0.92	15.5	0.85	0	*6.4*
58	0.98	13.1	0.90	11	*3.2*
60	0.92	6.1	0.79	24	*5.4*
61	0.95	3.2	0.79	31	*3.3*

(*) Mean absolute-value deviation between the best-fit and the experimentally measured relaxation rates (calculated over the set of 17 relaxation rates per residue).

(**) During the optimization procedure S_s^2 was constrained, $S_s^2 > 0.80$.

References

1. Shaka, A. J.; Keeler, J.; Frenkiel, T.; Freeman, R. *J. Magn. Reson.* **1983**, 52, 335-338.
2. Metz, G.; Wu, X. L.; Smith, S. O. *J. Magn. Reson. Ser. A* **1994**, 110, 219-227.
3. Baldus, M.; Geurts, D. G.; Hediger, S.; Meier, B. H. *J. Magn. Reson. Ser. A* **1996**, 118, 140-144.
4. Paulson, E. K.; Morcombe, C. R.; Gaponenko, V.; Dancheck, B.; Byrd, R. A.; Zilm, K. W. *J. Am. Chem. Soc.* **2003**, 125, 15831-15836.
5. Marion, D.; Wüthrich, K. *Biochem. Biophys. Res. Comm.* **1983**, 113, 967-974.
6. Chevelkov, V.; Rehbein, K.; Diehl, A.; Reif, B. *Angew. Chem. Int. Ed.* **2006**, 45, 3878-3881.
7. Eichmüller, C.; Skrynnikov N. R. *J. Biomol. NMR* **2005**, 32, 281-293.
8. Zilm, K. W. *Abstracts 48th ENC*, Daytona Beach, Florida, **2007**.
9. Kalk, A.; Berendsen, H. J. C.; *J. Magn. Reson.* **1976**, 24, 343-366.
10. Palmer, A. G.; Skelton, N. J.; Chazin, W. J.; Wright, P. E.; Rance, M. *Mol. Phys.* **1992**, 75, 699-711.
11. Sein, J.; Giraud, N.; Blackledge, M.; Emsley, L. *J. Magn. Reson.* **2007**, 186, 26-33.
12. Lipari, G.; Szabo, A. *J. Am. Chem. Soc.* **1982,** 104, 4546-4559.
13. Clore, G. M.; Szabo, A.; Bax, A.; Kay, L. E.; Driscoll, P. C.; Gronenborn, A. M. *J. Am. Chem. Soc.* **1990,** 112, 4989-4991. The specific parametrization used in here is from Skrynnikov, N. R.; Millet, O.; Kay, L. E. *J. Am. Chem. Soc.* **2002,** 124, 6449-6460.
14. Brooks, B. R.; Bruccoleri, R. E.; Olafson, B. D.; States, D. J.; Swaminathan, S.; Karplus, M. *J. Comput. Chem.* **1983**, 4, 187-217.
15. Buck, M.; Bouguet-Bonnet, S.; Pastor, R. W.; MacKerell, A. D. *Biophys. J.* **2006,** 90, L36-L38.
16. Yi, X.; Pavlova, M. S.; Ryabov, Y. E.; Reif, B.; Skrynnikov, N. R. *J. Am. Chem. Soc.* **2007**, 129, 6827-6838.
17. Li, H.; Robertson, A. D.; Jensen, J. H. *Proteins* **2005**, 61, 704-721.
18. Meinhold, L.; Smith, J. C. *Biophys. J.* **2005**, 88, 2554-2563.
19. Lienin, S. F.; Brüschweiler, R.; Ernst, R. R. *J. Magn. Reson.* **1998**, 131, 184-190.
20. Zeeb, M.; Jacob, M. H.; Schindler, T.; Balbach, J. *J. Biomol. NMR* **2003**, 27, 221-234.
21. Korchuganov, D. S.; Gagnidze, I. E.; Tkach, E. N.; Schulga, A. A.; Kirpichnikov, M. P.; Arseniev, A. S. *J. Biomol. NMR* **2004**, 30, 431-442.
22. Hall, D. A.; Maus, D. C.; Gerfen, G. J.; Inati, S. J.; Becerra, L. R.; Dahlquist, F. W.; Griffin, R. G. *Science* **1997**, 276, 930-932.
23. Gekko, K.; Timasheff, S. N. *Biochemistry* **1981**, 20, 4667-4676.
24. Betting, H.; Häckel, M.; Hinz, H. J.; Stockhausen, M. *Phys. Chem. Chem. Phys.* **2001**, 3, 1688-1692.
25. Caliskan, G.; Mechtani, D.; Roh, J. H.; Kisliuk, A.; Sokolov, A. P.; Azzam, S.; Cicerone, M. T.; Lin-Gibson, S.; Peral, I. *J. Chem. Phys.* **2004**, 121, 1978-1983.
26. Farrow, N. A.; Muhandiram, R.; Singer, A. U.; Pascal, S. M.; Kay, C. M.; Gish, G.; Shoelson, S. E.; Pawson, T.; Forman-Kay, J. D.; Kay, L. E. *Biochemistry* **1994**, 33, 5984-6003.
27. Korzhnev, D. M.; Skrynnikov, N. R.; Millet, O.; Torchia, D. A.; Kay, L. E. *J. Am. Chem. Soc.* **2002**, 124, 10743-10753.
28. Hansen, D. F.; Kay, L. E. *J. Biomol. NMR* **2007**, 37, 245-255.
29. Tjandra, N.; Feller, S. E.; Pastor, R. W.; Bax, A. *J. Am. Chem. Soc.* **1995**, 117, 12562-12566.
30. Lee, L. K.; Rance, M.; Chazin, W. J.; Palmer, A. G. *J. Biomol. NMR* **1997**, 9, 287-298.
31. Chen, J. H.; Brooks, C. L.; Wright, P. E. *J. Biomol. NMR* **2004**, 29, 243-257.